Fuel 224 (2018) 676–686

Contents lists available at ScienceDirect

Fuel

journal homepage: www.elsevier.com/locate/fuel

Steam reforming of tar model compounds over Ni/Mayenite catalysts: effect of Ce addition

E. Savuto[a,*], R.M. Navarro[b], N. Mota[b], A. Di Carlo[c], E. Bocci[d], M. Carlini[a], J.L.G. Fierro[b]

[a] Department of Agriculture, Forests, Nature and Energy (DAFNE), Tuscia University, via S. Camillo de Lellis, snc, 01100 Viterbo, Italy
[b] Instituto de Catálisis y Petroleoquímica (CSIC), Marie Curie 2, Cantoblanco, E-28049 Madrid, Spain
[c] Department of Industrial and Information Engineering and Economics, University of L'Aquila, Via Giovanni Gronchi 18, 67100 L'Aquila, Italy
[d] Marconi University, Via Plinio 24, Rome, Italy

ARTICLE INFO

Keywords:
Steam reforming
Tar
Nickel
Catalyst
Mayenite
Cerium

ABSTRACT

Ni-based catalysts are very effective and largely used for the steam reforming of heavy hydrocarbons (tars) generated from biomass gasification, even if Ni suffers from deactivation issues mainly due to carbon deposition, sintering and sulphur poisoning. Mayenite ($Ca_{12}Al_{14}O_{33}$), as support for Ni, has been previously studied and has shown excellent oxidation properties that increase the resistance of the catalyst to carbon deposits. Nevertheless Ni/Mayenite catalyst still suffers from sulphur poisoning. Ceria (CeO_2) is well known to be an effective promoter that can bring several advantages to catalysts, such as enhancing the resistance to carbon deposits and increasing the sulphur tolerance of nickel. Here CeO_2 is added to Ni/Mayenite catalysts to evaluate its promoting features and resistance to deactivation. In this study Ni/Mayenite and Ce/Ni/Mayenite catalysts were synthesized, characterized and tested in the steam reforming of tar model compounds. The catalytic tests were carried out under different operating parameters (temperature, space velocity and nature of tar compounds) and in the presence of sulphur, and the used samples were characterized to identify the reasons of deactivation.

1. Introduction

Biomass as a renewable energy source has become very interesting for its use in substitution of fossil fuels. As is widely known, biomass has several advantages such as being a CO_2-neutral energy source, being easily available and having a wide range of utilization or transformation processes. Among the possible processes, steam biomass gasification has attracted special attention because it allows to produce an H_2-rich producer gas utilizable for different applications such as combined heat and power production in co-generators [1], high efficiency electricity production in fuel cells [2], and biofuels production from Fischer-Tropsch synthesis and other processes [3–5]. However, in order to make this gas exploitable, it is fundamental to remove the pollutants generated during the gasification process. A gas cleaning and conditioning system is thus necessary for the removal of particulate and tars. In particular, tars are defined as the organics produced during the gasification process, generally assumed to be largely aromatic, that could condensate on piping and downstream devices, causing serious damages to the components of the plants [6,7]. As a result of this, the producer gas has to be treated with hot or cold conditioning systems. Typically, cold conditioning systems, like wet scrubbers [8], operate at temperatures close to ambient and involve mechanical methods or use of chemical solvents. However, wet scrubbers cause relevant thermal losses, due to their operation at ambient temperature, and originate waste streams (contaminated scrubbing liquids) difficult to dispose or recycle properly [9]. Hot conditioning systems instead focus mainly on catalytic conversion of tars at high temperature (close to gasification temperature of ~800 °C), which decompose the heavy hydrocarbons by means of steam reactions into H_2 and CO. This procedure allows the removal of tars and at the same time the enrichment of the gas with more fuel components (H_2 and CO). Furthermore, as the hot gas conditioning process operates at high temperature, there is the possibility to integrate it directly in the gasification reactor, as proposed and tested in the European Projects UNIQUE [10] and UNIfHY [11]. Rapagnà et al. [12,13] have indeed tested ceramic filter candles (Al_2O_3 based) impregnated with active phase (nickel) integrated inside the freeboard of a bench scale fluidized bed gasifier. The results obtained were very promising, showing a very high tar conversion rate (> 90%) for several hours and an increase of gas yield (from 1.0 to 2.09 Nm^3/kg) and H_2 content (from 39 to 56%) in the producer gas. The integration of catalytic tar conversion inside the freeboard of a fluidized bed gasifier has thus important advantages in terms of system compactness and

* Corresponding author.
E-mail address: savuto@unitus.it (E. Savuto).

https://doi.org/10.1016/j.fuel.2018.03.081
Received 10 October 2017; Received in revised form 6 March 2018; Accepted 13 March 2018

reduction of thermal losses [14–17]. For these reasons, research should be focused on finding an effective catalyst for tar steam reforming to be integrated inside the freeboard of a fluidized bed gasification reactor.

Among the catalysts suitable for steam reforming reactions at high temperatures, Ni-based catalysts are an interesting solution due to their good performance and moderate cost. Commercial Ni catalysts are often supported on alumina for its high surface area, but these kinds of catalysts are easily deactivated in tar steam reforming because of sintering [18], carbon deposition [19,20] and sulphur poisoning [21]. In particular, carbon deposition is a very relevant cause of degradation of nickel catalysts and therefore it has been widely studied and analysed in literature [19,20,22,23]. The Boudouard or disproportionation reaction ($2CO \leftrightarrow C + CO_2$; $\Delta H_{298\ K} = -172\ kJ\ mol^{-1}$) is considered, together with methane cracking, the main process responsible for the formation of carbon on the nickel surface and thus for the deactivation of the catalyst [24,25]. The deactivation issues can be avoided by changing some features of the catalyst; for instance sintering could be minimised by creating strong bounds between the active phase and the support, so that the Ni particles are not allowed to move and agglomerate on the catalyst surface [26]. The matter of carbon deposits on Ni catalysts has been widely studied [20,23,27–29] and some proposed solutions include the use of catalyst supports with high oxidative properties, in order to gasify/oxidise the carbon deposits thus protecting the active phase from carbon deactivation. Mayenite ($Ca_{12}Al_{14}O_{33}$) has a crystalline nanoporous structure with enhanced oxidative properties, due to its capacity to host free oxygen species (O_2^- and O_2^{2-}) in the cages of its lattice [30]. Mayenite has been used as support for Ni catalysts in the steam reforming of toluene as tar model compound [31] and also downstream a bench scale fluidized bed gasifier, thus working with a real gas containing a mixture of tars produced during a gasification process [32,33]. With toluene alone, Ni/Mayenite showed excellent performance with conversion around 100% in tests up to 60 h; in tests with addition of 500 ppm of H_2S the catalyst showed unchanged performance for the first 60 min, then the conversion dropped to approximately 70%, probably due to the deactivation of the catalyst caused by sulphur [31]. In presence of real syngas from gasification with approximately 100 ppm of H_2S, Ni/Mayenite also performed very well in the reforming of tars for 50 h, with conversion values close to 100% for all the compounds analysed; however it showed a sloped decrease in CH_4 conversion (80%–25%) after a few hours [33]. Again, this drop in the catalytic performance with time-on-stream was ascribed to the deactivation of Ni active phase by sulphur. Therefore, it has been demonstrated that mayenite is very effective in the prevention of carbon deposition on active Ni, but is not active against sulphur poisoning.

It is well known that the addition of ceria on Ni-based catalysts improves their activity and stability in the reforming of heavy tar compounds [34,35]. It has been reported that, thanks to its oxygen vacancies with high mobility [36], CeO_2 acts as an oxygen donor on the catalyst surface, promoting the reaction between CO_2 and C and thus helping to reduce carbon deposition by means of the reverse Boudouard reaction [37]. Furthermore, as suggested by Laycock et al. [24], Ce-promotion in presence of H_2S could increase, thanks to its excellent oxidative properties, the sulphur tolerance of Ni, thus reducing the poisonous effects of hydrogen sulfide on the Ni active sites.

In this work Ni/Mayenite and Ce/Ni/Mayenite catalysts have been studied in the steam reforming of tar model compounds at different operating conditions (temperature and space velocity). The resistance of the catalysts to sulphur poisoning was also evaluated in catalytic steam reforming tests performed using model feeds with added thiophene (C_4H_4S) as sulphur source.

2. Experimental

2.1. Catalysts preparation

Mayenite $Ca_{12}Al_{14}O_{33}$ was prepared by solid-state reaction, mechanically mixing calcium carbonate ($CaCO_3$) and alumina (Al_2O_3) in stoichiometric ratio ($CaCO_3/Al_2O_3 = 12/7$) [32,38–40]. Al_2O_3 was previously calcined in a muffle furnace at 850 °C for 5 h in order to remove some eventual moisture and impurities adsorbed on the surface, and also to stabilize it thermally before the synthesis of mayenite. The reactants, in the form of powder, were milled in a Planetary Ball Mill apparatus (Pulverisette-7, Fritsch) for 15 min at a speed of 450 rpm, in order to obtain a perfect mixture. The mixture was then calcined in a muffle furnace at 900 °C for 7 h in air atmosphere; the temperature was reached with a ramp of approximately 5 °C/min. The powder was then rehydrated and again calcined for the promotion of the complete synthesis of mayenite. It was found that the residual CaO after the first phase of preparation reacts in H_2O to form $Ca(OH)_2$ increasing its volume and releasing heat; these physical effects help to complete the synthesis of mayenite [41].

The Ni active phase was introduced by wetness impregnation using an aqueous solution of nickel nitrate hexahydrate ($Ni(NO_3)_2{\cdot}6H_2O$). The quantity of nickel nitrate was calculated in order to obtain 5% wt Ni on the catalyst. The solution, in which mayenite powder was added, was stirred and heated at 90 °C until it became slurry; then it was dried overnight at 120 °C and finally crushed in a mortar. The compound obtained was again calcined in a muffle furnace at 850 °C (higher than the operating temperature of the catalyst, in order to stabilize the Ni phase) for 5 h. The catalyst obtained with this procedure was denoted as Ni5M.

Part of the Ni5M obtained was then again impregnated with an aqueous solution of cerium nitrate hexahydrate ($Ce(NO_3)_3{\cdot}6H_2O$), in order to deposit 5% wt Ce on the catalyst. The procedure of wet impregnation with Ce was carried out analogously to the Ni impregnation; finally the compound was again calcined in a muffle furnace at 850 °C for 5 h [42,43]. The catalyst obtained with this procedure was denoted as Ce5Ni5M. The Ni5M and Ce5Ni5M powders were sieved between 200 and 425 μm for catalytic testing.

2.2. Catalysts characterization

For the identification of phases and crystallite dimension, fresh catalysts were characterized by means of X-ray Diffraction with a Seifert 3000P vertical diffractometer and nickel-filtered Cu Kα radiation ($\lambda = 0.1544$ nm) under constant instrument parameters. For each sample, Bragg angles between 10° and 80° were scanned. A rate of 0.02°/step, integration time 20 s/step were used during a continuous scan in the above mentioned range. The average crystallite sizes of NiO and CeO_2 were calculated by means of the Scherrer equation:

$$dp = \frac{K\lambda}{\beta cos\theta}$$

where λ is the X-ray wavelength, in this case 1.544 nm; β is the full width at half maximum height of the diffraction peak (FWHM); θ is the peak angle in radians, and K is a constant related to crystallite shape, taken as 0.9 [44].

Brunauer–Emmett–Teller (BET) specific surface area and Barrett-Joyner-Halenda (BJH) pore volume of the fresh catalysts were calculated from the results of the N_2 adsorption-desorption isotherms, measured at the N_2 liquid temperature of 77 K by means of a Micromeritics ASAP 2100 apparatus. The samples were degassed before the analysis at 393 K for 12 h to remove compounds possibly adsorbed on the surfaces.

The reducibility of the fresh catalysts was measured by means of Temperature Programmed Reduction (TPR) experiments in a Micromeritics TPD/TPR 2900 apparatus equipped with a TC detector. The samples were pre-treated under He at 100 °C for 30 min, then the TPR profiles were recorded by heating the sample from room temperature to 900 °C at a rate of 10 °C/min under a flow of H_2/He (10% v/v).

X-ray Photoelectron Spectroscopy (XPS) measurements were made on spent catalysts by means of a Fisons ESCALAB 200R spectrometer equipped with a hemispherical electron analyzer and an Al Ka ($h{\cdot}\nu = 1486.6$ eV, 1 eV = 1.6302×10^{-19} J) 120 W X-ray source.

The spent catalysts were characterized by thermogravimetric analysis with a TGA/SDTA 851e METTLER TOLEDO for the evaluation of the coke deposited on their surface after the activity tests. The temperature was raised from ambient to 900 °C with a heating rate of 10 °C/min in O_2 atmosphere (O_2 20%, 50 Nml/min), while the weight change was measured.

2.3. Catalytic activity tests

The activity tests were performed in a fixed bed stainless steel micro-reactor (I.D. 5.8 mm) placed in an electric furnace, in order to control and maintain the desired temperature for the reaction. Two thermocouples were used to measure the reaction temperature: one at the centre of the catalytic bed, and the second in contact with the external wall of the reactor. The catalytic bed consisted of the catalyst powder diluted with SiC (SiC/catalyst = 1.25/1) in order to maintain a constant temperature along the reactor and to avoid preferential gas paths. Both catalyst and SiC particle size were between 200 and 425 μm. Before reaction, the catalysts Ni5M and Ce5Ni5M were activated by reduction with H_2 flow (10% H_2, 90% N_2) while heating from ambient temperature to 800 °C, and for 1 h at constant temperature, in order to obtain metallic nickel (Ni^0) from nickel oxide (NiO).

Flows of N_2, H_2O and tar model compounds were introduced from the top of the reactor, previously passing through an evaporation section kept at 200 °C. The tar model compounds utilized in the tests were toluene (C_7H_8), naphthalene ($C_{10}H_8$) and thiophene (C_4H_4S). Toluene and naphthalene were chosen as representative model compounds of 1-ring and polyaromatics, respectively [45]; while thiophene was chosen as H_2S precursor because under reforming conditions produces H_2S, in concentration close (50–100 ppm) [46,47] to that observed during the biomass gasification process [16,33]. Furthermore, toluene has a very stable aromatic structure and is one of the major tar species [48,49] while naphthalene is representative of the heavy aromatics present in tars which are refractory to steam reforming [50,51].

Toluene was introduced in the reactor in liquid form, by means of a motorized syringe pump, while naphthalene and thiophene were dissolved in liquid toluene. The H_2O flow was controlled and sent to the evaporation section by means of a HPLC pump; the N_2 flow from the gas tank was measured and controlled with a mass flow controller. The total tar content in the gas mixture was set to 1.16% in agreement with experimental values obtained in a steam/air biomass gasifier [32,33,52]. The value of S/C molar ratio, fixed at approximately 4, was chosen because it corresponds to the ratio between the moles of steam and the moles of carbon contained in the tars of a typical producer gas composition obtained in a steam/air biomass gasification. Furthermore, as mentioned above, the aim of the tests is to find a catalyst to be integrated inside the biomass gasifier, therefore changes in the S/C ratio have not been considered because its value is established by the biomass gasifier. The total gas flow rate was 72 Nml/min, selected after preliminary tests to minimize diffusional resistances. Activity tests were carried out with different tar compounds: toluene alone, toluene and naphthalene, and finally toluene, naphthalene and thiophene in order to investigate the catalysts performances in presence of sulphur compounds (50 ppm). The toluene/naphthalene ratio (14/1) was selected taking into account the typical ratio between one-ring compounds and two or higher ring-compounds obtained in the tar analysis of a steam/air biomass gasifier [33].

Tests were carried out at different values of GHSV, by changing the quantity of catalyst charged in the reactor. At first, 5000 h^{-1} was chosen because it is the value recommended from the manufacturer of the ceramic catalytic candles designed to be inserted in the freeboard of the gasifier [12,14]. Then 20,000 h^{-1} was also selected, in order to reproduce industrial values of GHSV for steam reforming [53–55]; and finally 10,000 h^{-1} was also tested because it is widely used in literature as GHSV for biomass tar steam reforming [56–58].

Reaction temperature was selected at 800 °C, in order to reproduce the temperature in the freeboard of a fluidized bed gasifier, in which the catalyst would be inserted. 800 °C is indeed widely used as operating temperature in bubbling fluidized bed gasifiers [14,52,59]. Tests at lower temperature, 700 °C, were also performed in order to investigate the performance of the catalysts in case of temperature drops in some areas of the gasifier [60].

Downstream the reactor, the gas was sent to a cold trap kept at −10 °C in which residual H_2O and tars condensed in an impinger bottle filled with 2-propanol. Successively, the gas was sent to an on-line gas chromatograph (HP 5890 Series II) equipped with a TC detector for the analysis of the gases formed in the steam reforming reaction: H_2, CO, CO_2, CH_4 and light hydrocarbons (C2-C3). The catalysts were tested for approximately 9 h continuously on stream and the gas products were analysed periodically every 25 min, in order to record eventual changes in the gas composition during the progress of the reaction. From the analysis of the products at the outlet of the reactor, it was possible to calculate the gasification rate with the following formula:

$$Gasification\ (\%) = \frac{\sum molC_{prod,OUT}}{\sum molC_{tar,IN}} * 100$$

Blank experiments without catalysts were performed in order to know the contribution of the homogeneous gasification. On blank tests the gasification conversion was in all cases lower than 5%.

3. Results

3.1. Characterization of calcined catalysts

3.1.1. X-ray diffraction

The XRD patterns for Ni5M and Ce5Ni5M samples are displayed in Fig. 1. In both calcined catalysts it is possible to distinguish the typical reflections of crystalline $Ca_{12}Al_{14}O_{33}$, at 2θ angles of 18.0° and 33.2° that indicate the success of the synthesis process of the mayenite support [61]. It is possible that segregation of an excess of the Ca occurred during the preparation, since some reflections of crystalline CaO (37.2°, 53.7°) are observed in the diffractograms of both catalysts samples. The calcined catalysts also show the characteristic reflections of crystalline NiO at 43.1° and 63.3°. The sample Ce5Ni5M also shows reflections corresponding to crystalline CeO_2 (28.5°, 47.4°, 56.3°, 59.0°, 76.7°, 79.1°) in cerianite phase, formed after the cerium impregnation and calcination.

The average crystallite sizes were calculated from the main reflection peaks of NiO (43.2°) and CeO_2 (28.5°) by means of the Scherrer equation. The results obtained are displayed in Table 1. The crystalline size of NiO particles decreases after the impregnation with Ce, indicating a better dispersion of the active phase on the support, in line with previous studies reported in literature [62,63].

3.1.2. N_2 adsorption-desorption isotherms

The N_2 adsorption-desorption isotherms of Ni5M and Ce5Ni5M calcined catalysts are type IV, which correspond to mesoporous materials and are characteristic of a weak adsorbent-adsorbate interaction (see Fig. 1-S in Supplementary Material). The BET surface areas, calculated from N_2 adsorption-desorption isotherms, and pore volume, calculated from the BJH desorption isotherms of Ni5M and Ce5Ni5M, are listed in Table 2. From the textural results presented, it is observed that there is a slight increase in both surface area and pore volume in the sample Ce5Ni5M in relation to the Ni5M counterpart, which could be caused by the segregation of small entities of CeO_2 that could contribute to the observed increase of porosity in the catalyst.

3.2. Temperature programmed reduction

The hydrogen consumption curves obtained during the TPR analysis on Ni5M and Ce5Ni5M calcined samples are displayed in Fig. 2.

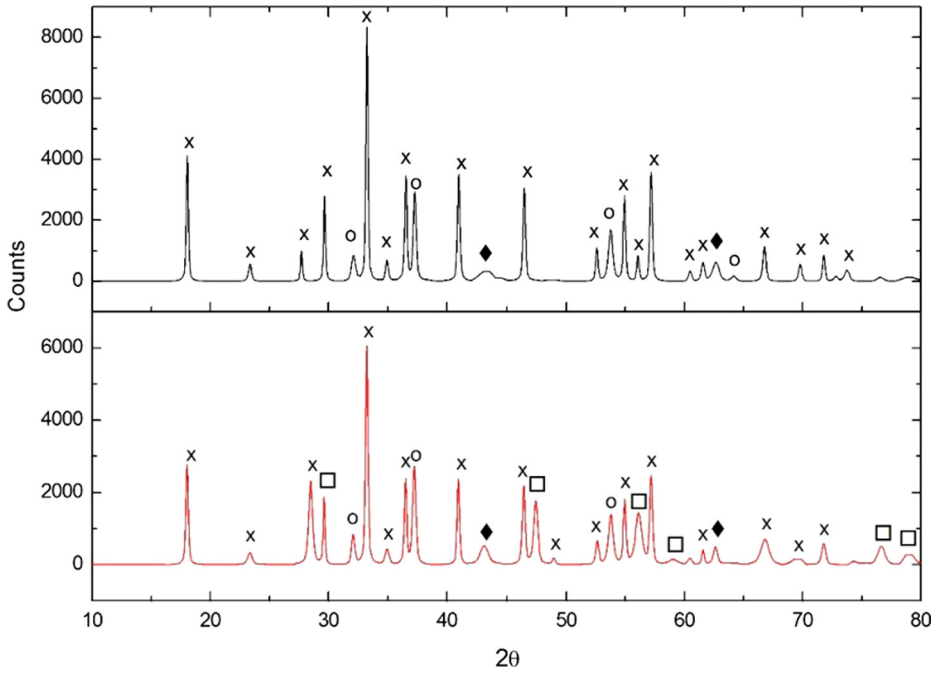

Fig. 1. XRD patterns of Ni5M (black) and Ce5Ni5M (red) calcined catalysts (x: $Ca_{12}Al_{14}O_{33}$, o: CaO, ♦: NiO, □: CeO_2). (For interpretation of the references to colour in this figure legend, the reader is referred to the web version of this article.)

Table 1
Crystallite size of NiO and CeO_2 particles from XRD in Ni5M and Ce5Ni5M calcined catalysts.

	Ni5M	Ce5Ni5M
Crystallite size (nm)		
NiO	21.9	18.8
CeO_2	–	28.0

Table 2
Textural properties obtained from N_2 adsorption-desorption isotherms of Ni5M and Ce5Ni5M calcined catalysts.

	BET surface area (m^2/g)	BJH Pore volume (cm^3/g)
Ni5M	20.7	0.112
Ce5Ni5M	24.3	0.143

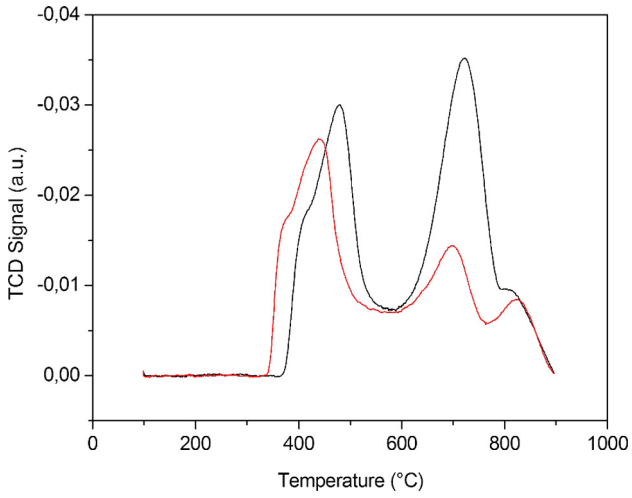

Fig. 2. Temperature-programmed reduction profiles of calcined Ni5M (black) and Ce5Ni5M (red) catalysts. (For interpretation of the references to colour in this figure legend, the reader is referred to the web version of this article.)

The reduction profiles of calcined samples show a similar profile at lower temperatures, with a first consumption peak around 440 °C for the Ce5Ni5M catalyst and around 480 °C for the Ni5M sample. In addition to these peaks, small shoulders at lower temperatures were also observed on both samples. The main reduction peaks observed at 440 and 480 °C could be ascribed to the reduction of free NiO particles to metallic Ni^0, which typically occurs at these temperatures [64–66], while the small shoulders could represent the reduction of some other NiO species with smaller particle size, easier to reduce and thus found at lower temperature. In the case of Ce5Ni5M, one can observe a shift towards lower temperature in the first reduction peak, indicative of an enhancement of the reducibility of NiO particles associated with the presence of CeO_2 in the catalyst formulation [67]. For higher temperatures, the TPR profiles of Ni5M and Ce5Ni5M calcined samples are quite different. In this region, the Ni5M sample presents a strong reduction peak at 722 °C, followed by a small shoulder at 810 °C. The reduction peak at 722 °C can be ascribed to the reduction of Ni^{2+} ions interacting at surface level with the Al-O of the mayenite support [68,69]. The area associated to the reduction of these Ni^{2+} species is the largest among the reduction peaks detected in the reduction profile of the Ni5M catalyst, indicating the fact that Ni bonded to the mayenite support by means of Al-O-Ni bonds are the prevalent Ni species in this catalyst. These Ni^{2+} ions strongly interact with the mayenite support, which protects them from the mobility and agglomeration with other Ni particles on the surface [26,28]. The last small reduction peak observed at 810 °C in the Ni5M profile could be ascribed to Ni^{2+} species interacting with Al_2O_3 segregated from the mayenite support during the Ni impregnation process. This effect was due to the wet impregnation carried out using an acid solution of $Ni(NO_3)_2$ which could extract some Al^{3+} ions from the structure of mayenite thus creating segregated Al_2O_3 particles on the surface of the support. By this way the Ni^{2+} ions could react with the surface of Al_2O_3 forming a spinel-like structure ($NiAl_2O_4$) that is reduced at approximately 800 °C [65,69,70]. The formation of $NiAl_2O_4$ takes place at the surface of Al_2O_3, not developing crystalline three-dimensional structures visible by XRD. The sample Ce5Ni5M shows in the high temperature range two reduction peaks at 700 and

820 °C, of lower intensity than those observed in the Ni5M counterpart. As it was indicated above for the Ni5M sample, the reduction peak at 700 °C can be ascribed to the reduction of Ni^{2+} ions bonded at surface level with the mayenite support. This peak also includes the reduction of bulk CeO_2 particles, because the reduction of these species is reported to occur in this temperature range [63,71]. The second reduction peak in the high temperature range observed at 820 °C could be attributed to the reduction of the spinel-like Ni species created by the interaction of Ni^{2+} ions with segregated Al_2O_3 species on the surface of the catalyst. The second reduction peak could be related to the second impregnation made with an acid solution of $Ce(NO_3)_3$, which could extract additional Al_2O_3 species on surface increasing by this way the concentration of the spinel-like Ni species. From the TPR profiles of the Ni5M and Ce5Ni5M catalysts, the reduction temperature for catalysts testing was set at 800 °C, in order to reduce an important proportion of the Ni^{2+} species with weak and high interaction with the mayenite support.

3.3. Catalytic activity tests

The effect of space velocity (GHSV = 5000, 10,000 and 20,000 h^{-1}) on the gasification capacity and selectivity to hydrogen production of the Ce5Ni5M catalyst, was firstly studied in the steam reforming of toluene at 800 °C (Fig. 3). The experimental points were fitted with trend lines and the coefficients of determination (R^2) are displayed in the diagrams. As derived from Fig. 3, the change of GHSV does not have a significant effect on the gasification conversion, resulting in similar values (close to 100%) under all the GHSV studied. Only a slight decrease in the slope of the average conversion was observed as the GHSV increased. The decrease in the gasification rate observed for higher space velocity was probably derived from the quicker deactivation of catalyst as consequence of the higher gas flow treated. The values of H_2/CO_x molar ratios are close to 1.57, irrespective of the GHSV studied, value typical for the toluene steam reforming ($C_7H_8 + 7H_2O \rightarrow 7CO + 11H_2$, $H_2/CO = 11/7 = 1.57$ [72]), showing a slight decrease with time-on-stream derived from the partial degradation of the catalyst. The small effect of the change in the GHSV on the catalytic behaviour of the Ce5Ni5M sample, led us not to implement similar tests on the Ce5Ni5M counterpart.

For the further catalytic tests, the value of GHSV was fixed at 10,000 h^{-1}, value widely used in tar steam reforming over Ni catalysts [56–58]. The results corresponding to the steam reforming of the

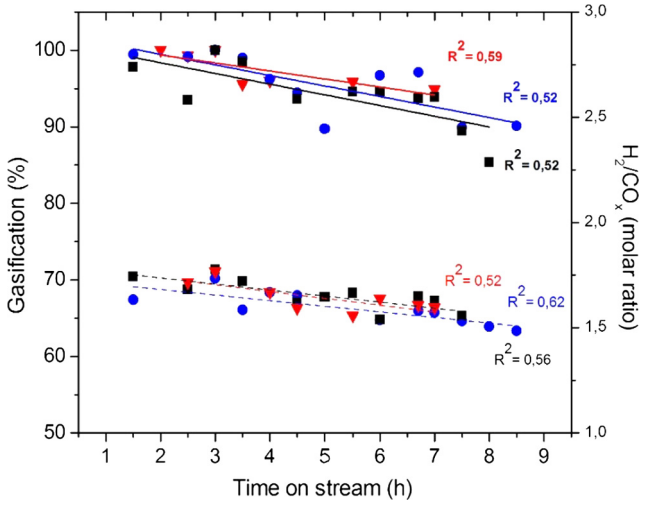

Fig. 3. Gasification conversion values and H_2/CO_x molar ratios in the steam reforming tests of toluene at 800 °C over the Ce5Ni5M catalyst at different GHSV: 20,000 h^{-1} (■), 10,000 h^{-1} (●) and 5,000 h^{-1} (▼).

mixture of toluene (T) and naphthalene (N) at this GHSV over the Ce5Ni5M and Ni5M catalysts at 800 °C are depicted in Fig. 4a. The conversion level in the steam reforming of the mixture of toluene and naphthalene over both catalysts also achieves an average gasification conversion around 100%, as it was previously observed in the reforming tests feeding only toluene (Fig. 3). The values of the H_2/CO_x molar ratio obtained in the reforming of the mixture of toluene and naphthalene are also close to the value for the complete stoichiometric steam reforming of both molecules (=1.57). The Ce5Ni5M and Ni5M catalysts show differences in their stability with time-on-stream in the reforming of the mixture (Fig. 4a). The average gasification conversion for Ni5M is very stable with time-on-stream, while for the Ce5Ni5M counterpart, the gasification rate decreases approximately 10% after 9 h of testing, indicating higher degradation for the catalyst containing Ce. The evolution of the H_2/CO_x ratio with time-on-stream follows the same trend observed in the gasification rate on these catalysts, that is higher stability for the Ni5M catalysts and slight decrease in the ratio for the Ce5Ni5M counterpart.

The steam reforming of the mixture of toluene and naphthalene over Ce5Ni5M and Ni5M was also performed at lower temperature (700 °C). The results corresponding to gasification conversion and the H_2/CO_x molar ratio obtained at this temperature are shown in Fig. 4b. As expected, the gasification conversion over the catalysts at this temperature is lower than the values obtained in the previous tests at 800 °C. It is observed that the reforming capacity of both catalysts at 700 °C is maintained during the first hours of reaction, decreasing suddenly after 5–6 h time-on-stream. To highlight the deactivation respect to the H_2/CO formation of the catalysts during the tests (Fig. 4b), trend lines have been added to experimental results to observe more clearly the evolution in the catalytic behaviour respect to their initial activity. The loss in the reforming capacity of the catalysts at 700 °C with time-on-stream could be related to a major participation of the CO disproportionation reaction (Boudouard reaction) with the decrease in the reactor temperature [28], which can cause higher carbon deposition and thus a drop in the reforming capacity [22]. Despite both catalysts showing deactivation, it is observed that the Ni5M catalyst showed better conversion and the fall in the reforming efficiency occurred later and more gradually, compared to the trend observed for Ce5Ni5M. The Ni5M catalyst shows gasification conversions around 80%, that decrease to around 30% after 7 h on stream. In the case of Ce5Ni5M, the initial gasification conversion begins with values between 80 and 70%, which drops to a value around 20% after 6 h on stream. The H_2/CO_x molar ratio follows a trend similar to that described for the reforming conversion, that is, stability in the first hours and sudden decrease after 5–6 h on stream.

The steam reforming of the mixture of toluene and naphthalene over Ce5Ni5M and Ni5M in presence of sulphur (thiophene 50 ppm) (S) was finally studied performing the tests at 800 °C with GHSV = 10,000 h^{-1}. The reforming results in presence of sulphur (Fig. 5) indicated that the reforming capacity of both catalysts decreased considerably in relation to the tests without sulphur (Fig. 4a). The gasification conversion values on both catalysts in the presence of sulphur show values around 15% with H_2/CO_x molar ratio around 0.25, decreasing both values slightly during the tests. The catalytic deactivation observed in presence of sulphur is probably caused by the sudden poisoning of the catalysts by the sulphur atoms contained in the thiophene present in the feed. From the results presented in Fig. 5a slightly higher conversion is observed on the Ce5Ni5M catalyst compared to the Ni5M counterpart. The better catalytic behaviour against sulphur observed in the sample Ce5Ni5M could be ascribed to the presence of CeO_2 in the catalytic formulation, which could protect some of the Ni active sites by promoting the oxidation of sulphur to SO_x, which has lower poisoning effect [73,74].

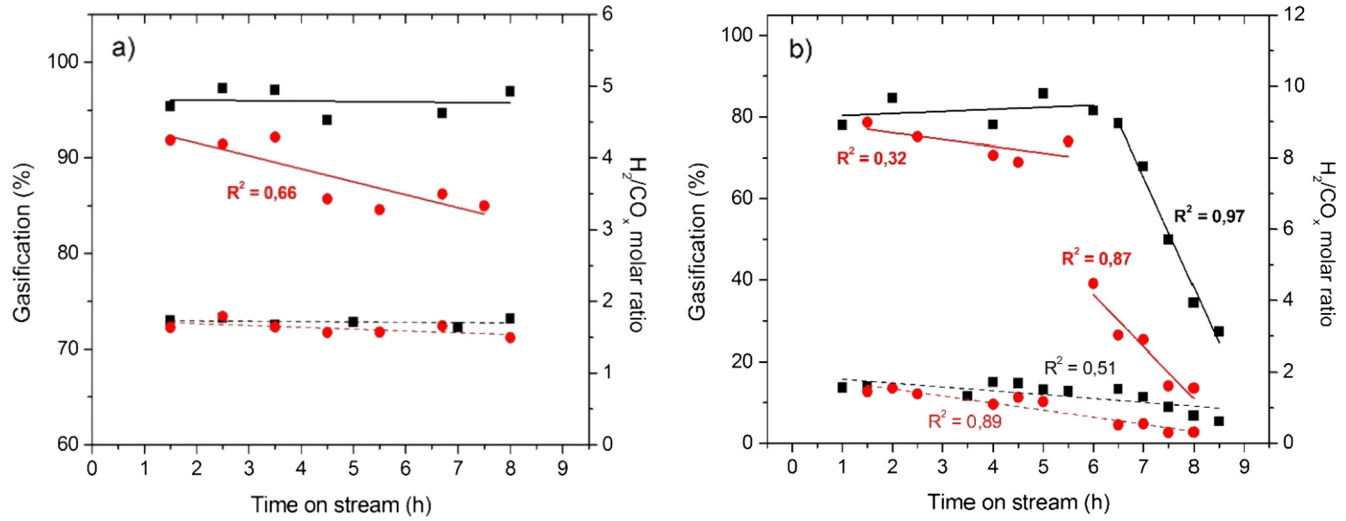

Fig. 4. Gasification conversion and H_2/CO_x molar ratios in the steam reforming tests of the mixture Toluene + Naphthalene at 800 °C (a) and 700 °C (b) over the Ni5M (■) and Ce5Ni5M (●) catalysts.

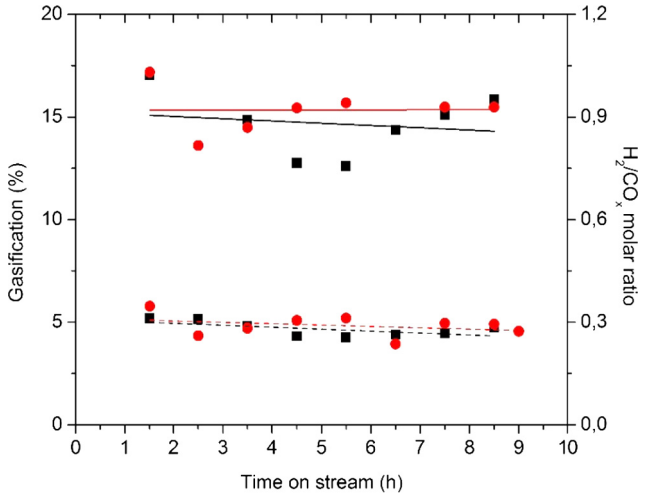

Fig. 5. Gasification conversion and H_2/CO_x molar ratios in the steam reforming tests of the mixture Toluene + Naphthalene + Thiophene over Ni5M (■) and Ce5Ni5M (●) catalysts.

3.4. Characterization of used catalysts

3.4.1. X-ray diffraction

The used catalysts were analysed by means of X-ray diffraction in order to investigate changes in their crystalline structure. Characterization of spent catalysts tested at different GHSVs (not shown here) did not show relevant structure changes, nor traces of carbon deposits on the catalysts derived from the reforming of toluene with different feed flows, as expected owing to the almost constant performance. The XRD profiles of the catalysts used in the steam reforming of the mixtures of Toluene and Naphthalene (T N) at 800 °C, T N at 700 °C, T N and thiophene (S) at 800 °C on Ce5Ni5M and Ni5M, are presented in Figs. 6 and 7 respectively. Diffractograms of used samples are quite similar to those presented of fresh samples, irrespective of the conditions of the reforming tests. The similarity of the XRD patterns before and after the tests means that the crystalline structure of the Ni, the support and the CeO_2 phases do not suffer significant changes during the catalytic tests, irrespective of the composition of the catalysts, the reforming temperature or the presence of sulphur in the feed. A more detailed analysis of the diffraction peaks appearing in the region around $2\theta = 26°$, characteristics of the presence of graphitic carbon structures (JCPDS 75–1621), indicated some differences in the profiles of the used catalysts samples. In this case, only in the catalysts used in presence of thiophene small diffraction peaks were observed which indicated the formation of graphitic or filamentous carbon structures on the surface of catalysts when the sulphur is present in the feed [29,75]. The higher formation of carbon structures observed in the catalysts when thiophene is present in the feed, could be related to the loss of the reforming capacity of the Ni phases due to the partial blocking of Ni, as a consequence of the poisoning with sulphur.

The size of the metallic Ni crystallites in the used catalysts, reported in Table 3, were calculated from the Scherrer equation applied to the (1 1 1) diffraction lines of metallic nickel at $2\theta = 44.8°$.

In almost all the used catalysts (except for the tests with thiophene), the Ce5Ni5M catalysts show large Ni crystallites after use, relevantly bigger than the Ni particles of the Ni5M counterpart. The crystallite growth of the Ce5Ni5M samples could be related to the lower quantity of Ni bond to the Al-O of the support compared to Ni5M, as remarked in the TPR results (see Fig. 2). The evolution of the Ni particle size under steam reaction conditions varies in the Ni5M and Ce5NiM samples. For the Ni5M catalyst, Ni growth was observed when the reforming was performed at low temperature and in the presence of sulphur. On the contrary, the Ni particles on the Ce5Ni5M samples show a lower sintering degree in the steam reforming performed with sulphur. In this case the partial blocking of Ni phases with sulphur could inhibit the sintering process [76] observed in the tests without sulphur in the feed.

3.5. Thermogravimetric oxidation

In Fig. 8 the derivatives of the TG-TPO profiles corresponding to the different catalysts used are depicted.

The DTG-TPO profiles for the Ce5Ni5M and Ni5M catalysts used in the steam reforming of toluene and naphthalene at 800 °C (GHSV 10,000 h^{-1}) are depicted in Fig. 8a. The DTG profiles are similar in the two used catalysts, showing three major peaks at around 220 °C, 400 °C and 650 °C. The peak at 220 °C, the major of the peaks detected, can be ascribed to the desorption of hydrocarbon species absorbed on the catalysts surface [77–79]. The peak at 400 °C (0.0358 mg), much lower than the previous (0.384 mg), could be ascribed to the oxidation of filamentous carbon species [23] and the last high peak appearing at 650 °C (0.174 mg) could be associated to the oxidation of graphitic carbon species, less reactive and thus oxidised at higher temperatures [27]. The oxidation profiles of the two used catalysts are similar, but with some differences in the intensity of the oxidation peaks. The Ce5Ni5M catalyst showed lower oxidation peaks at 220 and 400 °C compared to the Ni5M counterpart, while the oxidation peak at 650 °C

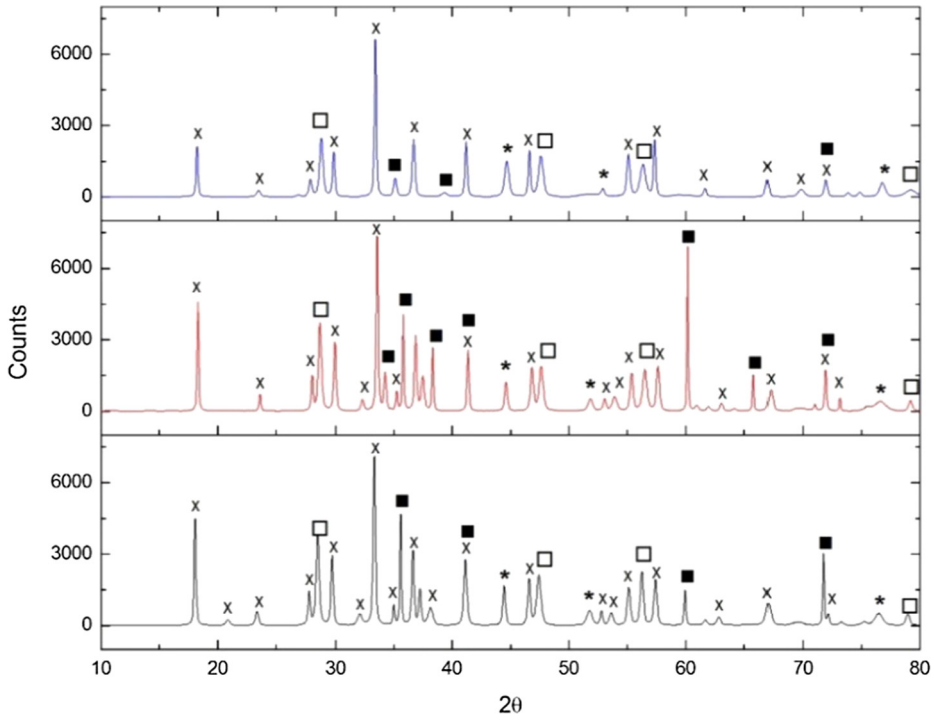

Fig. 6. XRD patterns of Ce5Ni5M used catalysts (black: T N; red: T N 700; blue: T N S); x: $Ca_{12}Al_{14}O_{33}$, ■: SiC, * : Ni, □: CeO_2). (For interpretation of the references to colour in this figure legend, the reader is referred to the web version of this article.)

corresponding to graphitic carbon was higher in the case of the Ce5Ni5M catalysts. It is possible that the bigger size of the Ni particles observed on the Ce5Ni5M catalysts (Table 3) reduces the amount of filamentous C species, which typically forms on small Ni particles. A higher amount of filamentous carbon species is indeed found on the Ni5M catalyst, probably associated with their smaller Ni particles. In addition to this, the oxidative properties of cerium species could also help in the removal of the species oxidised at low temperature. In the case of the production of graphitic carbon, the presence of Ce was not effective in reducing these types of carbon deposits on the catalyst surfaces.

The DTG-TPO profiles for the Ce5Ni5M and Ni5M catalysts used in the steam reforming of toluene and naphthalene at 700 °C (GHSV 10,000 h^{-1}) reported in Fig. 8b, displays the same three major

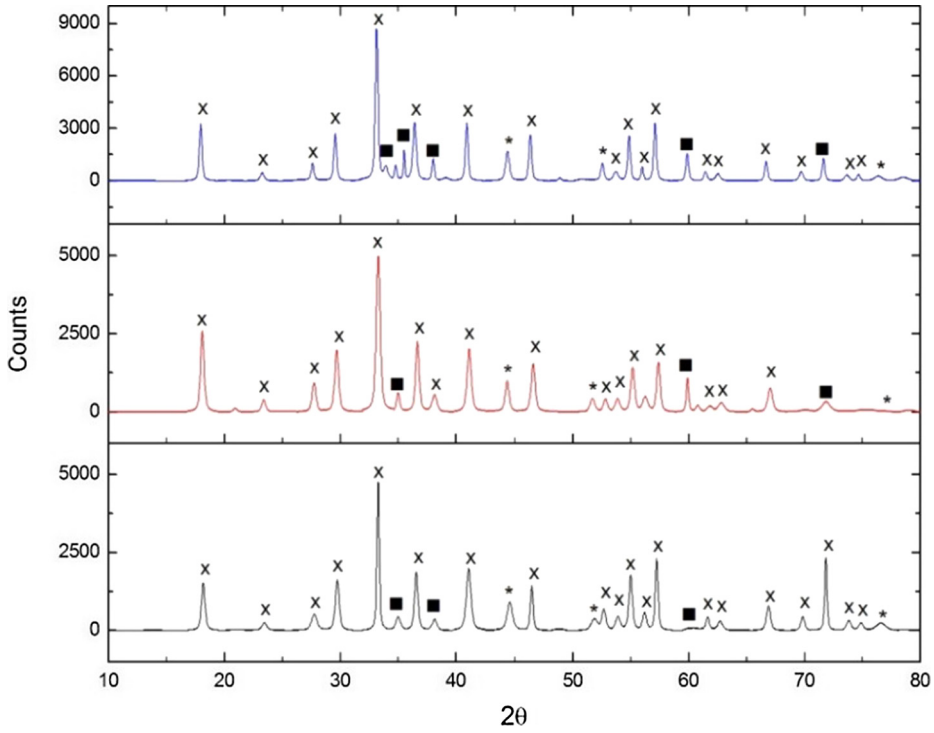

Fig. 7. XRD patterns of Ni5M used catalysts (black: T N; red: T N 700; blue: T N S; x: $Ca_{12}Al_{14}O_{33}$, ■:SiC, * : Ni). (For interpretation of the references to colour in this figure legend, the reader is referred to the web version of this article.)

Table 3
Average crystallite size of the Ni^0 particles detected on used catalysts from XRD.

	Ni Crystallite size (nm)
Ni5M T N	15.5
Ce5Ni5M T N	31.0
Ni5M T N 700	21.7
Ce5Ni5M T N 700	31.0
Ni5M T N S	21.7
Ce5Ni5M T N S	19.7

oxidation peaks at about 200, 400 and 650 °C, already described in the case of the catalysts used at 800 °C. Contrary to what was observed in the samples tested at 800 °C, in the samples tested at 700 °C the carbon deposits were mainly graphitic and thus inactive, difficult to remove and responsible for catalyst deactivation. The TGA results indicated therefore that the steam reforming of model compounds at 700 °C causes higher graphitic carbon deposition, probably due to the reaction of CO disproportionation [28,80], with consequent early deactivation of the catalyst and low catalytic performances. For the catalysts tested at 700 °C, the oxidation peak corresponding to filamentous carbon is lower for Ce5Ni5M in relation to the Ni5M counterpart as a consequence of the lower formation of small Ni particles when Ce is present in the catalyst formulation, as indicated above. In the case of the graphitic carbon (650 °C), a lower amount of carbon has deposited on the surface of Ce5Ni5M in relation to the Ni5M counterpart. It is possible that the lower quantity of graphitic carbon found on Ce5Ni5M is related to its lower reforming activity which can cause minor deposits of carbon on the surface of the catalyst.

The DTG-TPO profiles for the catalysts tested in the presence of thiophene are depicted in Fig. 8c. The oxidation profiles of the used Ce5Ni5M and Ni5M catalysts are very similar showing the oxidation peaks at around 200, 400 and 650 °C, already detected in the tests without thiophene. The oxidation peak at 650 °C is higher for Ce5Ni5M sample in relation to the Ni5M catalyst; this observation can be ascribed to the oxidative capacity of the cerium entities, that could reduce the formation of filamentous carbon species, but do not show capacity to remove the less reactive graphitic carbon species. The graphitic and filamentous carbon structures here identified could be associated to the diffraction peak at $2\theta = 26°$ detected in the XRD of the spent catalysts tested with thiophene. The higher carbon deposits found on these catalysts could be caused by the loss of the reforming capacity of the Ni active sites due to the sulphur poisoning. The quantity of carbon

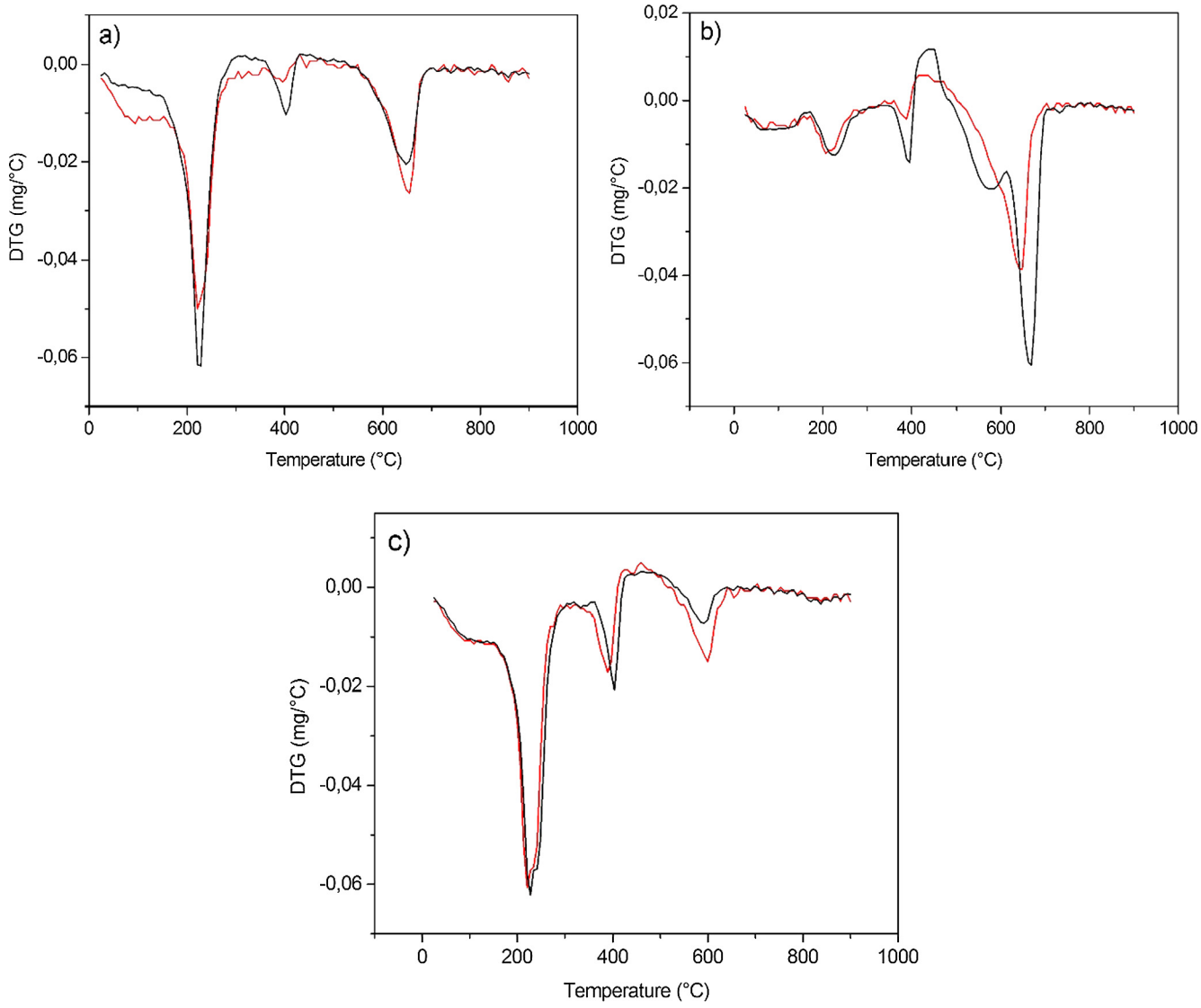

Fig. 8. DTG-TPO profiles of used catalysts Ce5Ni5M (red) and Ni5M (black) used in the steam reforming of (a) Toluene + Naphthalene at 800 °C; (b) Toluene + Naphthalene at 700 °C and (c) Toluene + Naphthalene + Thiophene at 800 °C. (For interpretation of the references to colour in this figure legend, the reader is referred to the web version of this article.)

deposited on used catalysts, in the form of filamentous and graphitic carbon (from 300 to 800 °C) in relation to the amount of hydrocarbon reacted, was calculated from the areas of the TGA-TPO profiles (values reported in Table 1S in Supplementary Material). The catalysts tested at 700 °C showed the highest extent of carbon deposition per unit gram of catalyst used. The carbon deposited per unit of hydrocarbon reformed show that Ni5M tested at 700 °C and with thiophene respectively are the catalysts with the highest carbon deposits. The Ce5Ni5M catalysts showed, in every case, lower carbon deposits on their surface compared to the Ni5M counterparts. The catalysts tested at 700 °C are more prone to carbon deposition, as explained before. Furthermore, the catalysts with addition of Ce show better resistance to carbon, even though their performance in promoting the steam reforming reactions is reduced.

3.6. X-ray photoelectron spectroscopy

The chemical state and composition of the used catalysts surfaces were evaluated by X-ray photoelectron spectroscopy (XPS). The binding energies of Ni2p$_{3/2}$, O1s, Ce3d$_{5/2}$ and S2p core-levels have been recorded for the used catalysts (results are summarized in Table 2S in Supplementary Material). For all used catalysts, the Ni 2p$_{3/2}$ level shows peaks at 852.3 and 855.3 eV; the peak at 852.3 eV corresponds to metallic Ni, while the peak at 855.3 eV is slightly higher than the binding energy of NiO (854.4 eV) and closer to the value of nickel aluminate (856.1 eV) [81,82]. This could be a consequence of the strong interaction between Ni^{2+} species and Al^{3+} ions from the support in the catalysts. The percentage values of the contributions to the Ni2p$_{3/2}$ level show that the Ni^{2+} is present in higher quantity compared to metallic Ni, suggesting that the Ni aluminate is the prevalent species on the surface of the catalysts. Differences in the percentage of metallic Ni are observed among the used samples, especially in the case of sample Ni5M tested at 700 °C, which does not show the presence of metallic nickel. The Ce3d$_{5/2}$ level on all Ce5Ni5M used catalysts was detected at a BE of 882.0 eV, characteristic of Ce^{4+} ions in CeO_2 species [83]. The presence of sulphur was only detected in the sample Ce5Ni5M used with thiophene. In this sample, the binding energy of the S2p level appears at 169.1 eV, typical of sulphate (SO_4^{2-}) species [84]. It is possible that the sulphate detected on the used samples could have been generated from the partial oxidation of S, taking into account the oxidation capacity of the cerium species.

The surface atomic concentration of the used catalysts has been calculated from the intensities of the XPS peaks normalized by atomic sensitivity factors; the results are summarized in Table 4.

The amount of surface nickel species was similar on the Ce5NiM and Ni5M catalysts, presenting some variations depending on the reforming conditions. A decrease in the concentration of the surface nickel species was observed when the reforming temperature increased from 700 °C to 800 °C with a further decrease when the reforming was performed in the presence of thiophene. There are not significant differences in the amount of carbon at surface level on used catalysts because this analysis includes, besides filamentous and graphitic carbon deposits quantified by TPO analysis, additional adsorbed hydrocarbon species which make it impossible to discern the differences previously observed in the TPO analyses. Sulphur was only detected in the sample Ce5Ni5M used with thiophene. The presence of sulphur in this sample could be related to the capacity of cerium species to adsorb and oxidise the H_2S to sulphate species [78–79]. The better catalytic behaviour observed for this sample against sulphur (Fig. 5) could be related to this fact, as it is known the lower poisoning effect of oxidized sulphur species could protect some of the Ni active sites from the poisoning of S^{2-} species.

Table 4
Surface atomic composition of used catalysts.

	Al (%at)	Ca (%at)	Ni (%at)	O (%at)	C (%at)	Ce (%at)	S (%at)
Ce5Ni5M T N	13.6	12.1	0.5	65.9	7.2	0.7	–
Ni5M T N	13.5	12.7	0.4	67.5	5.9	–	–
Ce5Ni5M T N 700	12.6	12.2	0.9	67.3	6.2	0.8	–
Ni5M T N 700	13.1	13.1	0.7	64.9	8.1	–	–
Ce5Ni5M T N S	18.7	13.4	0.4	60.6	6.1	0.7	0.1
Ni5M T N S	14.7	10.8	0.3	67.6	6.6	–	–

4. Conclusions

The performance of Ni/Mayenite catalyst promoted with CeO_2 has been studied in the steam reforming of tar model compounds (toluene, naphthalene and thiophene) at two different temperatures. The synthesis of mayenite and the Ni and Ce impregnations were successful, as demonstrated by the XRD patterns of the fresh catalysts. Characterization analysis showed that the addition of cerium to Ni/Mayenite enhances the surface area by increasing the porosity and also modifies the interaction degree of the Ni species with the mayenite support, leading to higher reducibility and a higher quantity of the Ni species bond to free Al_2O_3. The catalysts Ni/Mayenite (Ni5M) and Ce-Ni/Mayenite (Ce5Ni5M) were tested in the steam reforming of toluene and naphthalene at various operating conditions. Both catalysts performed well in the steam reforming of tar model compounds at 800 °C. Ce5Ni5M and Ni5M showed differences in their stability with time-on-stream. The average gasification rate for Ni5M was very stable with time-on-stream, while for Ce5Ni5M the gasification rate decreased approximately 10% after 9 h on stream, indicating higher degradation for the catalyst containing Ce. The reforming activity of both catalysts at 700 °C decreased suddenly after 5–6 h time-on-stream. At this lower reforming temperature, the Ni5M catalyst showed better performance, the decrease in efficiency occurred later and more gently compared to the Ce5Ni5M counterpart. In absence of sulphur, the Ce-containing catalyst decreases the reforming capacity of Ni/Mayenite, probably because the impregnation of Ce subsequent to the Ni incorporation could cover some Ni active sites. The reforming capacity of both catalysts drops dramatically with the presence of sulphur in the feed. The extremely low performance shown in this case is ascribed to the poisoning occurred on the Ni sites caused by the sulphur contained in thiophene. However in this case, the catalyst modified with cerium showed very slight increased reforming capacity in presence of sulphur compared to the behaviour of the unmodified Ni5M counterpart. The characterization of the used catalysts showed the formation of different carbon species on the surface of catalysts: adsorbed hydrocarbons, filamentous structures and graphitic carbon. Under all reforming conditions, the used catalysts modified with Cerium (Ce5Ni5M) showed lower extension on the carbon deposits (per g of catalyst) compared to the unpromoted Ni5M counterpart.

Acknowledgements

The authors thank the research programs supported by the Secretaría de Estado de Investigación, Desarrollo e Innovación and “Regional Government of Madrid” (Spain) under projects CTQ2016-76505-C3-1-R and S2013/MAE-2882, respectively. The authors also are grateful to Dr. Dalia Liuzzi from Instituto de Catálisis y Petroleoquímica (CSIC – ICP) for her help in the experimental activity and in the interpretation of the results.

Appendix A. Supplementary data

Supplementary data associated with this article can be found, in the online version, at http://dx.doi.org/10.1016/j.fuel.2018.03.081.

References

[1] Rodriguez Coronado C, Yoshioka JT, Silveira JL. Electricity, hot water and cold water production from biomass. Energetic and economical analysis of the compact

system of cogeneration run with woodgas from a small downdraft gasifier. Renew Energy 2011;36:1861–8. http://dx.doi.org/10.1016/j.renene.2010.11.021.
[2] Bocci E, Di Carlo A, McPhail SJ, Gallucci K, Foscolo PU, Moneti M, et al. Biomass to fuel cells state of the art: a review of the most innovative technology solutions. Int J Hydrogen Energy 2014;39:21876–95. http://dx.doi.org/10.1016/j.ijhydene.2014.09.022.
[3] Boerrigter H, Rauch R. Review of applications of gases from biomass gasification. ECN biomass. Coal Environ 2006;33.
[4] Sisinni M, Di Carlo A, Bocci E, Micangeli A, Naso V. Hydrogen-rich gas production by sorption enhanced steam reforming of woodgas containing TAR over a commercial Ni catalyst and calcined dolomite as CO2. Sorbent 2013:1–15. http://dx.doi.org/10.3390/en60x000x.
[5] Pallozzi V, Di Carlo A, Bocci E, Villarini M, Foscolo PU, Carlini M. Performance evaluation at different process parameters of an innovative prototype of biomass gasification amide to hydrogen production. Energy Convers Manag 2016.
[6] Milne TA, Evans RJ. Biomass gasifier "Tars": their nature, formation, and conversion. Constraints 1998. http://dx.doi.org/10.2172/3726.
[7] Shen Y, Yoshikawa K. Recent progresses in catalytic tar elimination during biomass gasification or pyrolysis – a review. Renew Sustain Energy Rev 2013;21:371–92. http://dx.doi.org/10.1016/j.rser.2012.12.062.
[8] Phuphuakrat T, Namioka T, Yoshikawa K. Absorptive removal of biomass tar using water and oily materials. Bioresour Technol 2011;102:543–9. http://dx.doi.org/10.1016/j.biortech.2010.07.073.
[9] Abdoulmoumine N, Adhikari S, Kulkarni A, Chattanathan S. A review on biomass gasification syngas cleanup. Appl Energy 2015;155:294–307. http://dx.doi.org/10.1016/j.apenergy.2015.05.095.
[10] UNIQUE Cooperative Research Project Contract N.211517 7FP; 2007. p. 1–96.
[11] UNIfHY Cooperative Research Project Contract N.299732 7FP; 2012.
[12] Rapagna S, Gallucci K, Di Marcello M, Foscolo PU, Nacken M, Heidenreich S. In situ catalytic ceramic candle filtration for tar reforming and particulate abatement in a fluidized-bed biomass gasifier. Energy Fuels 2009:3804–9.
[13] Rapagnà S, Gallucci K, Di Marcello M, Foscolo PU, Nacken M, Heidenreich S, et al. First Al2O3 based catalytic filter candles operating in the fluidized bed gasifier freeboard. Fuel 2012;97:718–24. http://dx.doi.org/10.1016/j.fuel.2012.02.043.
[14] D'Orazio A, Rapagnà S, Foscolo PU, Gallucci K, Nacken M, Heidenreich S, et al. Gas conditioning in H2 rich syngas production by biomass steam gasification: experimental comparison between three innovative ceramic filter candles. Int J Hydrogen Energy 2015;40:7282–90. http://dx.doi.org/10.1016/j.ijhydene.2015.03.169.
[15] Nacken M, Ma L, Engelen K, Heidenreich S, Baron G. Performance of a catalytically activated ceramic hot gas filter for catalytic tar removal from biomass gasification gas. Ind Eng Chem Res 2007.
[16] Nacken M, Ma L, Engelen K, Heidenreich S, Baron GV. Development of a tar reforming catalyst for integration in a ceramic filter element and use in hot gas cleaning. Energy Fuel 2007:1945–51.
[17] Di Carlo A, Foscolo PU. Hot syngas filtration in the freeboard of a fluidized bed gasifier: development of a CFD model. Powder Technol 2012;222:117–30. http://dx.doi.org/10.1016/j.powtec.2012.02.019.
[18] Sehested J. Sintering of nickel steam-reforming catalysts. J Catal 2003;217:417–26. http://dx.doi.org/10.1016/S0021-9517(03)00075-7.
[19] Rostrup-Nielsen J, Trimm DL. Mechanisms of carbon formation on nickel-containing catalysts. J Catal 1977;48:155–65. http://dx.doi.org/10.1016/0021-9517(77)90087-2.
[20] Trimm DL. Coke formation and minimisation during steam reforming reactions. Catal Today 1997;37:233–8. http://dx.doi.org/10.1016/S0920-5861(97)00014-X.
[21] Hepola J, Simell P. Sulphur poisoning of nickel-based hot gas cleaning catalysts in synthetic gasification gas I. Effect of different process parameters. Appl Catal B Environ 1997;14:287–303. http://dx.doi.org/10.1016/S0926-3373(97)00031-3.
[22] Bartholomew CH. Carbon deposition in steam reforming and methanation. Catal Rev Sci Eng 1982;24(1):67–112. http://dx.doi.org/10.1080/03602458208079650.
[23] Guo J, Lou H, Zheng X. The deposition of coke from methane on a Ni/MgAl2O4 catalyst. Carbon N Y 2007;45:1314–21. http://dx.doi.org/10.1016/j.carbon.2007.01.011.
[24] Laycock CJ, Staniforth JZ, Ormerod RM. Biogas as a fuel for solid oxide fuel cells and synthesis gas production: effects of ceria-doping and hydrogen sulfide on the performance of nickel-based anode materials. Dalton Trans 2011;40:5494. http://dx.doi.org/10.1039/c0dt01373k.
[25] Wang S, Lu GQ. Thermogravimetric analysis of carbon deposition over Ni/γ-Al_2O_3 catalysts in carbon dioxide reforming of methane. Energy & Fuels 1998:1235–40.
[26] Courson C, Udron L, Swierczynski D, Petit C, Kiennemann A. Hydrogen production from biomass gasification on nickel catalysts: tests for dry reforming of methane. Catal Today 2002;76:75–86. http://dx.doi.org/10.1016/S0920-5861(02)00202-X.
[27] Trimm DL. The formation and removal of coke from nickel catalyst. Catal Rev 1977;16:155–89. http://dx.doi.org/10.1080/03602457708079636.
[28] Bartholomew CH. Mechanisms of catalyst deactivation. Appl Catal A Gen 2001;212:17–60. http://dx.doi.org/10.1016/S0926-860X(00)00843-7.
[29] Liu BS, Au CT. Carbon deposition and catalyst stability over La_2NiO_4/γ-Al_2O_3 during CO_2 reforming of methane to syngas. Appl Catal A Gen 2003;244:181–95. http://dx.doi.org/10.1016/S0926-860X(02)00591-4.
[30] Hosono H, Abe Y. Occurrence of superoxide radical ion in crystalline calcium aluminate 12CaO.7Al_2O_3 prepared via solid-state reactions. Inorg Chem 1987;26:1192–5. http://dx.doi.org/10.1021/ic00255a003.
[31] Li C, Hirabayashi D, Suzuki K. A crucial role of O_2^- and O_{22}^- on mayenite structure for biomass tar steam reforming over Ni/$Ca_{12}Al_{14}O_{33}$. Appl Catal B Environ 2009;88:351–60. http://dx.doi.org/10.1016/j.apcatb.2008.11.004.
[32] Di Carlo A, Borello D, Sisinni M, Savuto E, Venturini P, Bocci E, et al. Reforming of tar contained in a raw fuel gas from biomass gasification using nickel-mayenite catalyst. Int J Hydrogen Energy 2015;40:9088–95. http://dx.doi.org/10.1016/j.ijhydene.2015.05.128.
[33] Savuto E, Di Carlo A, Gallucci K, Natali S, Bocci E. Characterization and performance analysis of an innovative Ni/Mayenite catalyst for the steam reforming of raw syngas. Fuel 2017;194:348–56. http://dx.doi.org/10.1016/j.fuel.2017.01.022.
[34] Alvarez-Galvan MC, Navarro RM, Rosa F, Briceño Y, Gordillo Alvarez F, Fierro JLG. Performance of La, Ce-modified alumina-supported Pt and Ni catalysts for the oxidative reforming of diesel hydrocarbons. Int J Hydrogen Energy 2008;33:652–63. http://dx.doi.org/10.1016/j.ijhydene.2007.10.023.
[35] Navarro RM, Guil-Lopez R, Ismail AA, Al-Sayari SA, Fierro JLG. Ni- and PtNi-catalysts supported on Al_2O_3 for acetone steam reforming: effect of the modification of support with Ce, la and Mg. Catal Today 2015;242:60–70. http://dx.doi.org/10.1016/j.cattod.2014.07.036.
[36] Wang S, Lu GQ. Role of CeO_2 in Ni/CeO_2-Al_2O_3 catalysts for carbon dioxide reforming of methane. Appl Catal B Environ 1998;19:267–77. http://dx.doi.org/10.1016/S0926-3373(98)00081-2.
[37] Bereketidou OA, Goula MA. Biogas reforming for syngas production over nickel supported on ceria-alumina catalysts. Catal Today 2012;195:93–100. http://dx.doi.org/10.1016/j.cattod.2012.07.006.
[38] Eufinger J-P, Schmidt A, Lerch M, Janek J. Novel anion conductors – conductivity, thermodynamic stability and hydration of anion-substituted mayenite-type cage compounds C 12 A 7: X (X = O, OH, Cl, F, CN, S, N). Phys Chem Chem Phys 2015;17:6844–57. http://dx.doi.org/10.1039/C4CP05442C.
[39] Ruszak M, Witkowski S, Pietrzyk P, Kotarba A, Sojka Z. The role of intermediate calcium aluminate phases in solid state synthesis of mayenite ($Ca_{12}Al_{14}O_{33}$). Funct Mater Lett 2011;4:183–6. http://dx.doi.org/10.1142/S1793604711001907.
[40] Ruszak M, Inger M, Witkowski S, Wilk M, Kotarba A, Sojka Z. Selective N_2O removal from the process gas of nitric acid plants over ceramic 12CaO•7Al_2O_3 catalyst. Catal Lett 2008;126:72–7. http://dx.doi.org/10.1007/s10562-008-9619-x.
[41] Martavaltzi CS, Lemonidou AA. Parametric study of the CaO-$Ca_{12}Al_{14}O_{33}$ synthesis with respect to high CO_2 sorption capacity and stability on multicycle operation. Ind Eng Chem Res 2008;47:9537–43. http://dx.doi.org/10.1021/ie800882d.
[42] Zhang R, Wang Y, Brown RC. Steam reforming of tar compounds over Ni/olivine catalysts doped with CeO2. Energy Convers Manag 2007;48:68–77. http://dx.doi.org/10.1016/j.enconman.2006.05.001.
[43] Zhuang Q, Chang L. Promoting effect of cerium oxide in supported nickel catalyst for hydrocarbon steam-reforming. Appl Catal 1991;70:1–8.
[44] Monshi A. Modified Scherrer equation to estimate more accurately nano-crystallite size using XRD. World J Nano Sci Eng 2012;2:154–60. http://dx.doi.org/10.4236/wjnse.2012.23020.
[45] Corella J, Caballero MA, Aznar M-P, Brage C. Two advanced models for the kinetics of the variation of the tar composition in its catalytic elimination in biomass gasification. Ind Eng Chem Res 2003;42:3001–11. http://dx.doi.org/10.1021/ie020401i.
[46] Rodriguez JA. Adsorption and decomposition of H_2S on MgO (100), NiMgO (100), and ZnO (0001) surfaces: a first-principles density functional study. J Phys Chem B 2000;104:3630–8.
[47] Rhyner U, Edinger P, Schildhauer TJ, Biollaz SMA. Experimental study on high temperature catalytic conversion of tars and organic sulfur compounds. Int J Hydrogen Energy 2014;39:4926–37. http://dx.doi.org/10.1016/j.ijhydene.2014.01.082.
[48] Kong M, Fei J, Wang S, Lu W, Zheng X. Influence of supports on catalytic behavior of nickel catalysts in carbon dioxide reforming of toluene as a model compound of tar from biomass gasification. Bioresour Technol 2011;102:2004–8. http://dx.doi.org/10.1016/j.biortech.2010.09.054.
[49] Swierczynski D, Courson C, Kiennemann A. Study of steam reforming of toluene used as model compound of tar produced by biomass gasification. Chem Eng Process Process Intensif 2008;47:508–13. http://dx.doi.org/10.1016/j.cep.2007.01.012.
[50] Furusawa T, Tsutsumi A. Development of cobalt catalysts for the steam reforming of naphthalene as a model compound of tar derived from biomass gasification. Appl Catal A 2005;278:195–205. http://dx.doi.org/10.1016/j.apcata.2004.09.034.
[51] Bampenrat A, Meeyoo V, Kitiyanan B, Rangsunvigit P, Rirksomboon T. Naphthalene steam reforming over Mn-doped CeO2-ZrO2 supported nickel catalysts. Appl Catal A Gen 2010;373:154–9. http://dx.doi.org/10.1016/j.apcata.2009.11.008.
[52] De Andrés M, Narros A, Rodríguez ME. Air-steam gasification of sewage sludge in a bubbling bed reactor: effect of alumina as a primary catalyst. Fuel Process Technol 2011;92:433–40. http://dx.doi.org/10.1016/j.fuproc.2010.10.006.
[53] Zhai X, Ding S, Liu Z, Jin Y, Cheng Y. Catalytic performance of Ni catalysts for steam reforming of methane at high space velocity. Int J Hydrogen Energy 2011;36:482–9. http://dx.doi.org/10.1016/j.ijhydene.2010.10.053.
[54] Josuinkas FM, Quitete CPB, Ribeiro NFP, Souza MMVM. Steam reforming of model gasification tar compounds over nickel catalysts prepared from hydrotalcite precursors. Fuel Process Technol 2014;121:76–82. http://dx.doi.org/10.1016/j.fuproc.2014.01.007.
[55] Yamazaki O, Tomishige K, Fujimoto K. Development of highly stable nickel catalyst for methane-steam reaction under low steam to carbon ratio. Appl Catal A Gen 1996;136:49–56. http://dx.doi.org/10.1016/0926-860X(95)00268-5.
[56] Corella J, Orío A, Toledo JM. Biomass gasification with air in a fluidized bed: exhaustive tar elimination with commercial steam reforming catalysts. Energy Fuels 1999;13:702–9. http://dx.doi.org/10.1021/ef980221e.
[57] Bangala DN, Abatzoglou N, Chornet E. Steam reforming of naphthalene on Ni-Cr/Al_2O_3 catalysts doped with MgO, TiO_2, and La_2O_3. AIChE J 1998;44:927–36. http://dx.doi.org/10.1002/aic.690440418.
[58] Łamacz A, Krztoń A, Djéga-Mariadassou G. Steam reforming of model gasification tars compounds on nickel based ceria-zirconia catalysts. Catal Today

2011;176:347–51. http://dx.doi.org/10.1016/j.cattod.2010.11.067.
[59] Rapagnà S, Virginie M, Gallucci K, Courson C, DiM Kiennemann A, et al. Fe/olivine catalyst for biomass steam gasification: preparation, characterization and testing at real process conditions. Catal Today 2011;176:163–8. http://dx.doi.org/10.1016/j.cattod.2010.11.098.
[60] Barisano D, Canneto G, Nanna F, Alvino E, Pinto G, Villone A, et al. Steam/oxygen biomass gasification at pilot scale in an internally circulating bubbling fluidized bed reactor. Fuel Process Technol 2016;141:74–81. http://dx.doi.org/10.1016/j.fuproc.2015.06.008.
[61] Tolkacheva AS, Shkerin SN, Plaksin SV, Vovkotrub EG, Bulanin KM, Kochedykov VA, et al. Synthesis of dense ceramics of single-phase mayenite (Ca12Al14O32)O. Russ J Appl Chem 2011;84:907–11. http://dx.doi.org/10.1134/S1070427211060012.
[62] Meng F, Li Z, Liu J, Cui X, Zheng H. Effect of promoter Ce on the structure and catalytic performance of Ni/Al2O3 catalyst for CO methanation in slurry-bed reactor. J Nat Gas Sci Eng 2015;23:250–8. http://dx.doi.org/10.1016/j.jngse.2015.01.041.
[63] Koo KY, Roh HS, Jung UH, Yoon WL. Combined H_2O and CO_2 reforming of CH_4 over Ce-promoted Ni/Al_2O_3 catalyst for gas to liquid (GTL) process: enhancement of Ni-CeO_2 interaction. Catal Today 2012;185:126–30. http://dx.doi.org/10.1016/j.cattod.2011.07.027.
[64] Xu P, Zhou Z, Zhao C, Chen Z. Ni/CaO-Al_2O_3 bifunctional catalysts for sorption-enhanced steam methane reforming. AIChE J 2014;60:3547–56. http://dx.doi.org/10.1002/aic.
[65] Roh H, Jun K, Dong W, Park S, Joe Y. Partial oxidation of methane over Ni/θ-Al_2O_3 catalysts. Chem Lett 2001:666–7. http://dx.doi.org/10.1246/cl.2001.666.
[66] Di Giuliano A, Girr J, Massacesi R, Gallucci K, Courson C. Sorption enhanced steam methane reforming by Ni-CaO materials supported on mayenite. Int J Hydrogen Energy 2016:1–20. http://dx.doi.org/10.1016/j.ijhydene.2016.11.198.
[67] Ashok J, Kawi S. Steam reforming of toluene as a biomass tar model compound over CeO_2 promoted Ni/CaOeAl_2O_3 catalytic systems. Int J Hydrogen Energy 2013;38:13938–49. http://dx.doi.org/10.1016/j.ijhydene.2013.08.029.
[68] Zheng W, Zhang J, Ge Q, Xu H, Li W. Effects of CeO_2 addition on Ni/Al_2O_3 catalysts for the reaction of ammonia decomposition to hydrogen. Appl Catal B Environ 2008;80:98–105. http://dx.doi.org/10.1016/j.apcatb.2007.11.008.
[69] Cai X, Cai Y, Lin W. Autothermal reforming of methane over Ni catalysts. J Nat Gas Chem 2008;17:201–7.
[70] Elias KFM, Lucrédio AF, Assaf EM. Effect of CaO addition on acid properties of Ni-Ca/Al_2O_3 catalysts applied to ethanol steam reforming. Int J Hydrogen Energy 2013;38:4407–17. http://dx.doi.org/10.1016/j.ijhydene.2013.01.162.
[71] Charisiou ND, Siakavelas G, Papageridis KN, Baklavaridis A, Tzounis L, Avraam DG, et al. Syngas production via the biogas dry reforming reaction over nickel supported on modified with CeO2 and/or La2O3 alumina catalysts. J Nat Gas Sci Eng 2016;31:164–83. http://dx.doi.org/10.1016/j.jngse.2016.02.021.
[72] Li C, Hirabayashi D, Suzuki K. Steam reforming of biomass tar producing H2-rich gases over Ni/MgOx/CaO1-x catalyst. Bioresour Technol 2010;101:97–100. http://dx.doi.org/10.1016/j.biortech.2009.03.043.
[73] Pacheco Gómez FJ. Mechanism of sulfur poisoning by H_2S and SO_2 of nickel and cobalt based catalysts for dry reforming of methane; 2016.
[74] Galea NM, Lo JMH, Ziegler T. A DFT study on the removal of adsorbed sulfur from a nickel(111) surface: reducing anode poisoning. J Catal 2009;263:380–9. http://dx.doi.org/10.1016/j.jcat.2009.03.001.
[75] Li ZQ, Lu CJ, Xia ZP, Zhou Y, Luo Z. X-ray diffraction patterns of graphite and turbostratic carbon. Carbon N Y 2007;45:1686–95. http://dx.doi.org/10.1016/j.carbon.2007.03.038.
[76] Sehested J, Gelten JAP, Remediakis IN, Bengaard H, Nørskov JK. Sintering of nickel steam-reforming catalysts: effects of temperature and steam and hydrogen pressures. J Catal 2004;223:432–43. http://dx.doi.org/10.1016/j.jcat.2004.01.026.
[77] Tomishige K, Chen Y, Fujimoto K. Studies on carbon deposition in CO_2 reforming of CH over nickel – magnesia solid solution catalysts. J Catal 1999;181:91–103.
[78] Koike M, Hisada Y, Wang L, Li D, Watanabe H, Nakagawa Y, et al. High catalytic activity of Co-Fe/Al_2O_3 in the steam reforming of toluene in the presence of hydrogen. Appl Catal B Environ 2013;140–141:652–62. http://dx.doi.org/10.1016/j.apcatb.2013.04.065.
[79] Bengaard HS, Nørskov JK, Sehested J, Clausen BS, Nielsen LP, Molenbroek AM, et al. Steam reforming and graphite formation on Ni catalysts. J Catal 2002;384:365–84. http://dx.doi.org/10.1006/jcat.2002.3579.
[80] Zhang Z, Verykios XE. Carbon dioxide reforming of methane to synthesis gas over Ni/La2O3 catalysts. Appl Catal A Gen 1996;138:109–33. http://dx.doi.org/10.1016/0926-860X(95)00238-3.
[81] Iriondo A, Barrio VL, Cambra JF, Arias PL, Guemez MB, Sanchez-Sanchez MC, et al. Glycerol steam reforming over Ni catalysts supported on ceria and ceria-promoted alumina. Int J Hydrogen Energy 2010;35:11622–33. http://dx.doi.org/10.1016/j.ijhydene.2010.05.105.
[82] Czekaj I, Loviat F, Raimondi F, Wambach J, Biollaz S, Wokaun A. Characterization of surface processes at the Ni-based catalyst during the methanation of biomass-derived synthesis gas: X-ray photoelectron spectroscopy (XPS). Appl Catal A Gen 2007;329:68–78. http://dx.doi.org/10.1016/j.apcata.2007.06.027.
[83] Kobayashi Y, Fujiwara Y. Chemical deposition of cerium oxide thin films on nickel substrate from aqueous solution. J Alloys Compd 2006;412:1157–60. http://dx.doi.org/10.1016/j.jallcom.2004.12.115.
[84] Bukhtiyarova GA, Bukhtiyarov VI, Sakaeva NS, Kaichev VV, Zolotovskii BP. XPS study of the silica-supported Fe-containing catalysts for deep or partial H 2 S oxidation. J Mol Catal A Chem 2000;158:251–5.